

Dual-polarization Dirac cones in a simple 2D square lattice photonic crystal

J. A. RODRÍGUEZ,*  B. WANG, AND M. A. CAPPELLI

Department of Mechanical Engineering, Stanford University, Stanford, California 94305-3032, USA

*Corresponding author: jrodrig@stanford.edu

Received 27 January 2020; revised 6 March 2020; accepted 23 March 2020; posted 24 March 2020 (Doc. ID 389163); published 20 April 2020

We report on dual-polarization Dirac cones in a simple square lattice two-dimensional (2D) photonic crystal (PC) based on transmission at accidental degeneracies centered at the $k = 0$ symmetry (Γ) point. Finite difference time domain simulations are used to identify the material and geometric parameters for Dirac-like dispersion. A configuration that produces a Dirac-like point for both transverse electric and transverse magnetic polarizations at the same frequency is presented. The PC dispersion shows the expected threefold degenerate linear branch crossings at the Dirac-like point. Full-field electromagnetic wave simulations exhibit some common behaviors of devices based on Dirac-like dispersion, such as cloaking and waveguiding. The configuration works for a considerable range of the parameter space, and thus is experimentally realizable with a wide range of materials. © 2020 Optical Society of America

<https://doi.org/10.1364/OL.389163>

It has been shown that two-dimensional (2D) dielectric photonic crystals (PCs) of square lattice symmetry have Dirac-like points (DPs) based on accidental degeneracies that result in Dirac cone dispersion at a frequency about the Brillouin zone center, i.e., the $\Gamma = 0$ symmetry point [1]. In the vicinity of a DP of this nature, the dispersion varies from a negative to positive refractive index, passing through zero [2]. At such a point, there exists a triple degeneracy between three propagation modes of the crystal, and incident electromagnetic (EM) waves are presented with an effective medium that behaves as a zero index metamaterial (ZIM) with a simultaneous zero effective permittivity ($\epsilon_{\text{eff}} = 0$) and permeability ($\mu_{\text{eff}} = 0$). Inside the medium, the wavelengths are “stretched,” and the fields are electrostatic, and the exact shape of the boundary of the medium becomes irrelevant [3]. Furthermore, the impedance at the interface between vacuum and such a medium is finite, unlike a zero-epsilon medium with a finite permeability, where the infinite impedance results in poor wave penetration. The EM behavior of a ZIM that utilizes DPs leads to many phenomena and applications that make DPs an active subject of study, such as cloaking or waveguiding, seen below in Fig. 1. In Fig 1(a), we show the transverse magnetic (TM) wave dispersion for a square lattice consisting of dielectric rods (dielectric constant, $\epsilon = 8.9$) having a ratio of radius r to lattice constant a of $r/a = 0.22$.

In the right frame [Fig. 1(b)], EM wave simulations confirm the ability of this medium to both cloak an embedded object, and also the waveguide, through successive 90 deg bends.

Up until recently, these types of PC devices based on Dirac-like dispersion have operated predominantly in TM polarization, where the magnetic field vector of the EM wave is directed across the rods that make up the PC. However, DPs in PCs with square lattice symmetry have also been shown to appear and produce the same effects for the transverse electric (TE) polarization where the electric field vector of the EM wave is oriented across the rods [4]. Furthermore, the DPs exploited to give rise to the cloaking and waveguiding behavior often correspond to degeneracies of the three lowest-order modes, resulting in the ZIM behavior pictured in Fig. 1, where the entirety of the PC has the same phase. However, in cases where field modes of high order are involved or the DP does not occur at the Γ point, the medium can give rise to complex phase structures within it while still redirecting phase fronts in a useful manner and behaving similar to a ZIM due to the coherent superposition of the three Bloch propagating modes [5]. Similar work has also been presented on PCs with hexagonal symmetry where even low-order DPs give rise to complex phase structures but still result in the behavior that makes DPs a topic of continued interest [6].

In this work, we identify a square lattice PC configuration that exhibits Dirac-like dispersion in both TM and TE polarizations at the same frequency, heretofore referred to as a dual-polarization Dirac point (DPDP). Using computational simulations, DPDPs have been realized in PCs by embedding a dielectric material in elliptic metamaterials [7], by engineering the accidental degeneracies in 3D PCs composed of a cubic array of core-shell structures [8], and via topology optimization, which leads to complex gradients in dielectric constant throughout the unit cell [9]. Our approach represents a simpler and more experimentally realizable configuration when compared to these previous examples, as our design simply calls for the use of rods of a uniform, isotropic ϵ in a 2D square lattice. We do not impose a strong constraint on the value of ϵ , and, as described below, DPDPs can be obtained over a range of ϵ spanning those of commonly available dielectrics.

A diagram showing the geometry of our PC is found in Fig. 2. The size, spacing, and material properties of the rods are determined by parameter searches within an EM finite difference

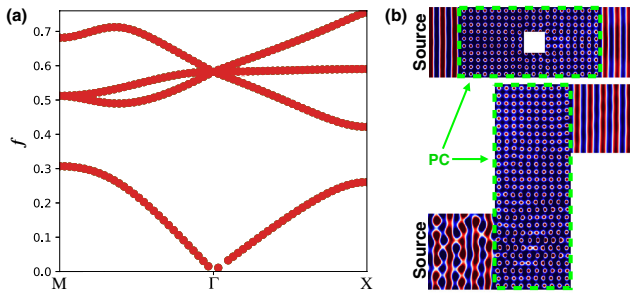


Fig. 1. (a) Typical dispersion diagram and (b) corresponding field behavior at the Dirac-like point in the TM polarization at $r/a = 0.22$ and $\varepsilon = 8.9$, exhibiting both cloaking and waveguiding. The frequency axis in (a) is nondimensionalized by lattice frequency, c/a .

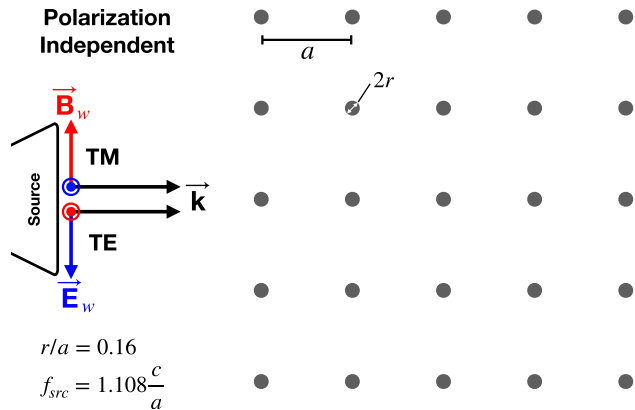


Fig. 2. Schematic of the PC cloak configuration where the axis of the cylindrical elements is oriented out of the page.

time domain (FDTD) simulation, the MIT Electromagnetic Equation Propagation (MEEP) solver [10]. This software is used to locate the DPs in the 3D parameter space of dielectric constant ε , frequency f , and radius to lattice spacing ratio r/a . It is important to note that due to the high frequencies and higher-order modes present in most of the DPs found, effective medium theory cannot be used to calculate the effective permittivity and permeability of the crystal [11]. Since we are utilizing accidental degeneracies, an overlap of DPs from both polarizations in the 3D parameter space is quite rare and was obtained via parameter sweeps and manual tuning. The values of r/a and ε were first varied over a wide range of values ($r/a \in [0, 0.5]$ and $\varepsilon \in [5, 12]$), and each dispersion diagram produced was examined for the presence of DPs. Dispersion structures that closely resembled DPs were further tuned, making sure that characteristics that verify the presence of Dirac-like dispersion like band inversion and linear branch crossings were observed. Once the eigensolver collapses to a single solution at the DP frequency at $\mathbf{k} = 0$, the configuration is considered sufficient to produce the desired behavior. Once the parameter sweep was finished and several DPs were discovered, their trajectories through the 3D parameter space were mapped by steadily varying the parameter values for each DP. The point presented in this work is a point at which DP trajectories in the 3D parameter space for TE and TM polarizations intersect.

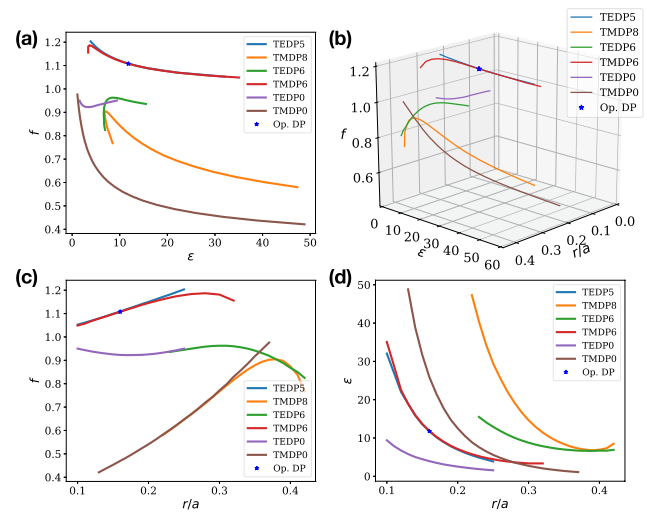


Fig. 3. Trajectories of selected DPs through the relevant parameter space. DPs are labeled according to the lowest of the three modes that are degenerate at the DP. In addition to the 3D perspective in the top right (b), projections onto the (a) $f - \varepsilon$, (c) $f - r/a$, and (d) $\varepsilon - r/a$ planes are presented. The operating DP occurs at $(r/a, \varepsilon, f) = (0.16, 11.8, 1.108)$.

Prior to the above parameter search, a resolution study was carried out using MEEP. While fixing the material parameters and lattice spacing, the resolution of the simulation was incrementally increased. After each resolution increase, the dispersion diagram was checked for any changes. It was determined that any increase in resolution above 150 (MEEP units) did not change the qualitative attributes of the dispersion structure at all and would at most affect the frequency values output by the eigensolver on the order of $\pm 10^{-5} c/a$. Thus, this resolution was chosen and used for all dispersion diagrams and full-field simulations to ensure consistent results. Furthermore, this means that the DP coordinates identified in this study are within a small neighborhood of the true values, and lie within any reasonable experimental tolerances for microwave devices.

As a result of the parameter sweep, many unique DPs were discovered, where a unique DP corresponds to the crossing of three specific modes in the PC dispersion. For example, the DP at $(r/a, \varepsilon, f) = (0.22, 8.9, 0.582)$ and the DP at $(r/a, \varepsilon, f) = (0.3, 2.73, 0.771)$ both correspond to the crossing of the zeroth-, first-, and second-order modes at $k = 0$ for the TM polarization, so they are considered to be two points on the trajectory of the same DP. DPs discovered at lower frequencies $\sim 1c/a$ or less were selected for further investigation due to their higher likelihood of good cloaking performance, and their full 3D trajectories were mapped. Full-field simulations of DPs at higher frequencies showed poor performance due to the scale of the PC elements being too close to or larger than the wavelength scale. The trajectories for selected DPs are plotted in Fig. 3.

Of the selected trajectories, it appears that DPs travel through the 3D parameter space in much the same way, however, not in an entirely predictable manner. For example, the DP for the TM polarization that results from the degeneracy of the 8th-, 9th-, and 10th-order modes (TMDP8; the DPs are named according to the lowest-order mode that is degenerate at the DP) appears to have an additional inflection point in its trajectory compared to TMDP0. In each of the 2D projections in

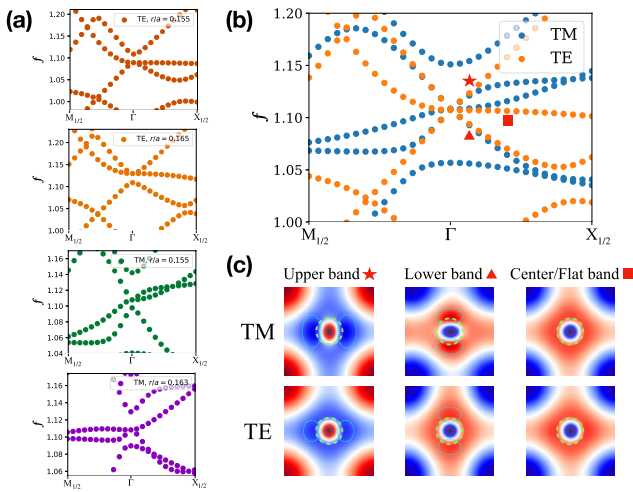


Fig. 4. (a) Band diagrams for both polarizations in the vicinity of the DP in r/a space, where it is evident from the dispersion topology that band inversion occurs. (b) Dispersion diagram showing the overlap of TMDP6 and TEDP5 where the linear branches cross at the same point in both the TE and TM polarizations. (c) E_z and H_z fields plotted for TM and TE polarizations, respectively, in a single unit cell, showing the three DP field modes at $\mathbf{k} = 0.0167\hat{\mathbf{x}}$, where the bands are denoted by the red shapes in the dispersion diagram. Thick green dashed lines denote the locations of the dielectric rods in the unit cell, and cyan dashed lines outline lobes of high field intensity that flank the rod. $M_{1/2}$ refers to $\mathbf{k} = 0.25\hat{\mathbf{x}} + 0.25\hat{\mathbf{y}}$, and $X_{1/2}$ similarly refers to $\mathbf{k} = 0.25\hat{\mathbf{x}}$ in normalized reciprocal space.

Fig. 3, the similarity of the trajectories of the DPs is more easily observed. There does not seem to be a qualitative difference in how DPs of either polarization travel through the parameter space. The near-pass between TMDP8 and TEDP6 does not result in good dispersion topology for the full-field behavior that is desired when parameters in between the two trajectories at their closest point are selected. The overlap between TEDP5 and TMDP6, in contrast, does lead to the field behavior that we desire over a considerable range of the parameter space, as the two trajectories are nearly on top of one another in the ranges of $r/a \in (0.13, 0.21)$, $f \in (1.07, 1.16)$, and $\varepsilon \in (5, 22)$. This means that in principle one could choose any one of a range of materials when constructing the polarization-independent device. For example, the dielectric constant $\varepsilon = 11.8$ is typical of that of silicon or a high-grade alumina. If we construct the PC out of alumina rods with lattice constant 1 cm, then we would use 0.16 cm radius alumina rods, and the DPs (for TE and TM) would be at $1.108 \times 3 \times 10^{10}$ Hz, or 33.24 GHz. This point, which is near the middle of the range above (the blue star in the figure), is selected, and its full-field behavior is investigated. A dispersion diagram showing the coincident DPs in both polarizations is shown in Fig. 4.

At the operating DP specified above, we see field behavior very similar to a ZIM, with a few key differences. First, the modes that are degenerate at the DP are not the typical monopole and dipole modes present at DPs of lower order as can be seen in Fig. 4. Instead, the modes appear to be strongly monopolar within the dielectric rod, with the upper and lower bands exhibiting lobes of high field intensity that flank the rod. In general, the field modes present are fairly complicated and

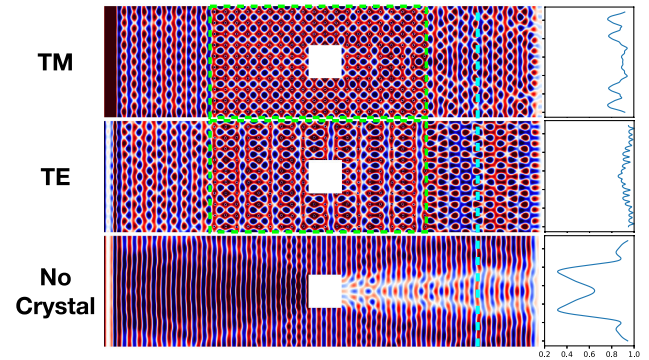


Fig. 5. Full-field simulation showing cloaking performance at the operating DP. H_z is plotted for TE, and E_z is plotted for TM where $\hat{\mathbf{z}}$ is out of the page. The PC is outlined by the green dashed line, while the cyan dashed line denotes the plane at which the relative intensity profiles on the right are sampled. Each profile is normalized by the maximum intensity reached in the TE polarization. The upper and lower boundaries as well as the defects are the perfect electric conductor or perfect magnetic conductor for the TE and TM polarizations, respectively.

multipolar. The PC can also be configured to cloak with interesting results shown in Fig. 5. As can be observed in the figure, the magnitude of the EM wave is preserved directly downstream of the square object embedded in the cloak, leading to the near complete removal of the wake behind the object, much like a ZIM. Because the normalized operating frequency is ~ 1 , the wavelength of the waves is comparable in scale to the lattice spacing of the PC. As a consequence, the phase fronts of the outgoing light contain defects on the same scale as the PC structure. Thus, this “cloaking” device has a signature of its presence, and, in addition, there will be variation in the outgoing signal as the size of the defect is varied. However, even for objects that obstruct a large portion of the wave’s path, the bulk of the energy of the EM wave is directed around the object as if it is not there.

This operating DP can also be used to mirror the waveguiding behavior alluded to before, as shown in Fig. 6. In the figure, the output signal has a uniform intensity profile similar to the cloaking case in Fig. 5 after two 90 deg turns with sharp corners. Both of these full-field simulations reproduce the key field behaviors that are expected at DPs as shown in Fig. 1 with the caveat that the phase fronts exiting the device carry a signature of the PC lattice. This device would therefore be useful in carrying bulk signals around defects in the material and around bends regardless of the polarization of the signal, leading to more versatility. In addition, the DPDP also allows for the use of circularly polarized light. A PC device composed of plasma rods similar to that featured in prior work [12] that has an externally applied magnetic field could utilize the configuration described in this paper to operate over a range of frequencies by tuning the plasma density and external magnetic field [13]. The material dispersion of the magnetized plasma allows the PC elements to attain any value of ε as long as right-circularly polarized light is used. The construction of the PC out of gaseous plasmas allows for rapid switching and reconfiguration—a property generally not attainable with dielectric rods. This and other unique devices can be designed using the polarization-independent Dirac-like dispersion presented here.

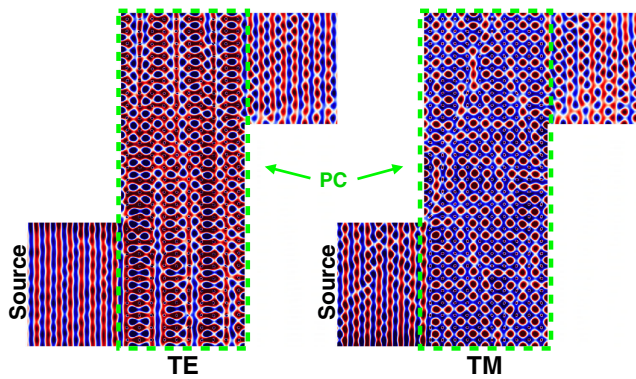


Fig. 6. Full-field simulation showing waveguiding performance at the operating DP. H_z is plotted for TE, and E_z is plotted for TM where \hat{z} is out of the page. The PC is outlined by the green dashed line. The boundaries are the perfect electric conductor or perfect magnetic conductor for the TM and TE polarizations, respectively.

Future research includes a number of tasks and opportunities. For example, the main limitation of the performance of this configuration is due to the high frequency at which the DP exists. Mapping of more DP trajectories could lead to a crossing at a lower frequency $f < 1$, which would likely lead to the output signal being fully reconstructed without phase defects. Toward this end, instead of manually sweeping and tuning parameters as before, a machine learning (ML) model may be able to predict the trajectories of the accidental degeneracies. Prior parameter sweeps amount to what is essentially a large labeled dataset, which could, in principle, be used to train a ML model to find the locations of new DPs and predict the trajectories of known DPs in the 2D square lattice PC system. In addition, this work is likely to generalize to PCs with other lattice symmetries, such as the hexagonal lattice in Ref. [6], where more overlapping accidental degeneracies may exist. In the absence of a new, lower frequency configuration, the device presented here could also be demonstrated experimentally with a range of materials using the validation procedure presented by Dong *et al.* [14].

In conclusion, we present a device that exhibits Dirac-like dispersion for both TE and TM polarizations with the DP having the same frequency in both polarizations. The operating DPDP was identified by tracking a number of DPs through the relevant 3D parameter space while searching for a point at which a TE

DP and TM DP overlap in their trajectories. The operating DPDP exhibits some of the key behaviors typical of DPs for both polarizations, including waveguiding and cloaking where the wake behind an object is almost entirely eliminated. The configuration functions for a wide range of dielectric constants and thus could be realized experimentally with several materials.

Funding. Air Force Office of Scientific Research (FA9550-14-1-0317); Department of Energy Computational Science Graduate Fellowship via the Krell Institute (DE-GF02-97ER25308).

Acknowledgment. This research was supported by a Multidisciplinary University Research Initiative from the Air Force Office of Scientific Research, with Dr. Mitat Birkan as the program manager. J. A. R. acknowledges support from the Krell Institute DOE Computational Science Graduate Fellowship.

Disclosures. The authors declare no conflicts of interest.

REFERENCES

1. X. Huang, Y. Lai, Z. H. Hang, H. Zheng, and C. T. Chan, *Nat. Mater.* **10**, 582 (2011).
2. L. G. Wang, Z. G. Wang, J. X. Zhang, and S. Y. Zhu, *Opt. Lett.* **34**, 1510 (2009).
3. D. I. Vulis, O. Reshef, P. Camayd-Muñoz, and E. Mazur, *Rep. Prog. Phys.* **82**, 012001 (2018).
4. Y. Chen, F. Meng, G. Li, and X. Huang, *Acta Mater.* **164**, 377 (2019).
5. H. F. Gao, X. Zhang, F. G. Wu, Y. W. Yao, and J. Li, *Solid State Commun.* **234–235**, 35 (2016).
6. M. Minkov, I. Williamson, M. Xiao, and S. Fan, *Phys. Rev. Lett.* **121**, 263901 (2018).
7. J. Wang, X. Chen, F. Zhao, and J. Dong, *Sci. Rep.* **6**, 22739 (2016).
8. C. T. Chan, X. Huang, F. Liu, and Z. Hang, *Prog. Electromagn. Res. B* **44**, 163 (2012).
9. Z. Lin, L. Christakis, Y. Li, E. Mazur, A. Rodriguez, and L. Lončar, *Phys. Rev. B* **97**, 081408 (2018).
10. A. F. Oskooi, D. Roundy, M. Ibanescu, P. Bermel, J. D. Joannopoulos, and S. G. Johnson, *Comput. Phys. Commun.* **181**, 687 (2010).
11. C. T. Chan, Z. H. Hang, and X. Huang, *Adv. Optoelectron.* **2012**, 313984 (2012).
12. B. Wang and M. A. Cappelli, *AIP Adv.* **6**, 065015 (2016).
13. J. Rodriguez, B. Wang, and M. A. Cappelli, *72nd Annual Gaseous Electronics Conference* (2019), paper FT1.00011.
14. G. Dong, J. Zhou, X. Yang, and X. Meng, *Sci. Rep.* **6**, 36712 (2016).